# Differences in the Location of Guest Molecules within Zeolite Pores As Revealed by Multilaser Excitation Confocal Fluorescence Microscopy: Which Molecule Is Where?

Christoph Sprung and Bert M. Weckhuysen*

Inorganic Chemistry and Catalysis, Department of Chemistry, Faculty of Science, Utrecht University, Universiteitsweg 99, 3584 CG Utrecht, The Netherlands

Ⓢ Supporting Information

ABSTRACT: A detailed and systematic polarized confocal fluorescence microscopy investigation is presented on three batches of large coffin-shaped ZSM-5 crystals (i.e., parent, steamed at 500 °C, and steamed at 700 °C). In total, six laser lines of different wavelength in the visible region are employed on two crystal positions and three orientations with respect to the polarization plane of the excitation laser light. A fluorescent probe molecule is generated inside the zeolite pores, originating from the acid-catalyzed oligomerization of 4-fluorostyrene. A thorough analysis of the polarization plane of emitting fluorescent light reveals insight into the orientation of the fluorescent probe molecule restricted by the highly ordered zeolite channel framework, thereby visualizing pore accessibility and clearly distinguishing the occupation of straight and sinusoidal channels by the probe molecule. Spectral features are, furthermore, observed to tell apart molecules situated in one or the other pore. Special focus was given on the rim and tip regions of the zeolite ZSM-5 crystals. On the basis of the confocal approach of the investigation, the aforementioned features are evaluated in three dimensions, while the degradation of the zeolite framework upon postsynthesis steam treatment could be visualized by occupation of the sinusoidal pores.
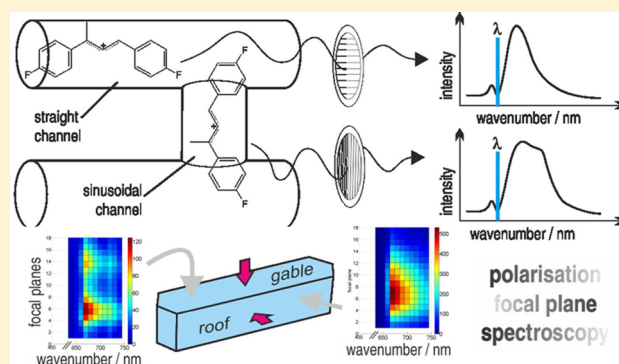
1. INTRODUCTION

Zeolites are an important group of heterogeneous catalysts. The various pore architectures of zeolites give these catalyst materials unique properties for shape selectivity toward reactants, products, and transition states.[1,2] Combination with catalytic activity makes zeolites relevant catalysts for chemical processes, such as isomerization, alkylation, and cracking reactions. Fluid catalytic cracking (FCC) is a central process in petrochemistry in which zeolites, such as zeolite Y and ZSM-5, are utilized.[3]

It is of high interest to develop structure–reactivity relationships for such zeolites. Investigations have, therefore, been carried out on model systems, such as coffin-shaped ZSM-5 crystals.[4−10,13,14] These crystals are composed of six subunits and have proven to be ideal for detailed microscopic investigations due to their micrometer size, as shown in the schematic drawing of Figure 1. Their long axis is surrounded by four rectangular pyramidal subunits, whose tips join in the very center of the crystal—the rectangular bases form the outer surface. The top and bottom subunits fill the remaining inner volume, and roof-like top forms the surface on either end of the long axis. A detailed structural investigation was recently presented by Ristanovic et al.,[15] who performed μXRD experiments to determine the crystallographic structure of each single subunit. Their common crystallographic c axis was
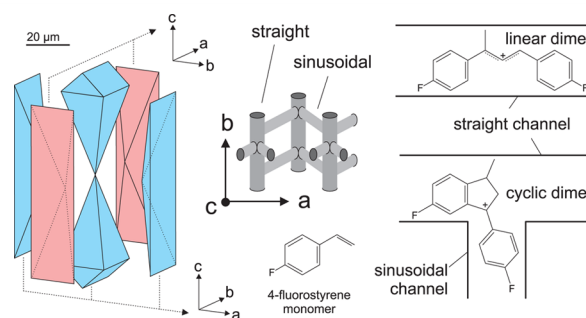
Figure 1. Large coffin-shaped ZSM-5 crystal: The model shows the six subunits and the internal pore architecture for sinusoidal and straight pores. A 4-fluorostyrene monomer is shown in the lower center, which was used to create linear and cyclic fluorescent dimeric carbocations, illustrated on the right side inside the ZSM-5 channel framework.

parallel to the crystals' long axis, and the four pyramidal subunits had an identical crystallographic orientation when being opposite, and it was 90° rotated for neighboring units. This structural relationship was also confirmed by polarized light microscopy[16] and EBSD/SEM[17,18] investigations.

The model in Figure 1 is therefore a 2-component model. Also, a 3-component model has been proposed for coffin-shaped ZSM-5 crystals, in which an additional subunit is located in the very center of the crystal. Roeffaers et al. suggest this 3-component model to be the preferred one for coffin-shaped ZSM-5 crystals.[19] The crystal structure of ZSM-5 was monoclinic and orthorhombic before and after addition of probe molecules, respectively, such as, e.g., styrene derivates.[20]

The adsorption of probe molecules inside the channel framework of ZSM-5 has proven to be a useful methodology to investigate the reactivity of these samples.[6,21] UV–vis absorption microspectroscopy reveals spectral features of the products formed inside the zeolite pores.[4,6] Styrene derivates, as will be used in our investigation, form both cyclic and linear dimeric carbocation species, with absorption bands at around 490 and 580 nm, respectively.[22] The exact numbers depend on the type of styrene derivate.[6] The thermodynamics of this proposed oligomerization reaction mechanism[22] were followed by DFT calculations.[23] Zeolite ZSM-5 has a three-dimensional (3-D) internal pore network, consisting of narrow straight and sinusoidal channels with sizes of 5.3 × 5.6 Å and 5.1 × 5.5 Å,[24,25] respectively. Straight channels are running along the crystallographic b vector, i.e., [010], and sinusoidal channels are perpendicular along the a vector, i.e., [100].[15] Molecules, which are adsorbed in those channels are, therefore, strictly oriented. Also, the diffusion properties are influenced by the internal channel network; Caro et al. followed the uptake of n-hexane in large coffin-shaped ZSM-5 crystals with a microbalance and found a three times higher diffusion coefficient perpendicular to the crystal's long axis compared to diffusion parallel to it,[26] which was confirmed by interference microscopy imaging.[27]

Absorption and emission of light are polarization-dependent processes. In particular, the degree of alignment of the transition dipole moment vector (of a specific molecule) with the polarization plane of the incoming light determines the intensity of absorption. The reverse process (i.e., emission), therefore, releases plane-polarized light. This anisotropic spectroscopic information was related to structural characteristics of such ZSM-5 crystals for absorption spectroscopy[4,9,27–30] and emission spectroscopy.[9,31,32] Roeffaers et al.[31,32] were able to record activity maps for furfuryl alcohol condensation inside ZSM-5 crystals (supported by EBSD investigations), where they found the rim to be the most active toward this reaction. Additionally, they observed the molecules in the center of the top and bottom subunits to be aligned perpendicular to the surface, whereas the molecules in the reactive rim were aligned parallel to the surface and the short axis of the crystal.

The origin of polarized fluorescence microscopy can be found in the field of life sciences, e.g., the location, molecular orientations, and behavior inside lipid and cell membranes[33] (with excellent reviews and chapters describing this field in more detail[30,34–42]). It is, however, also a highly attractive methodology to investigate molecules inside zeolite pores.[43–46]

Therein, zeolite L is of great interest for, e.g., the absorption of dyes for laser applications.[47] The one-dimensional channels in the crystalline structure of zeolite L provide an ideal architecture to investigate molecular orientation and interaction (through fluorescence live time measurements).[47–49] Huber et al. employed this type of zeolite to determine the polarization of various fluorescence bands of dye molecules.[50] Megelski et al. observed the orientation of three different dye molecules inside zeolite L. The largest of those (i.e., POPOP) could only

be oriented along the direction of the zeolite channels, whereas oxonine and pyronine were able to be positioned with half cone angles up to 40° and 30° with respect to the channel direction.[44] Furthermore, the location and orientation of molecules inside zeolite channels was observed by multiplex coherent anti-Stokes Raman scattering (mCARS).[29,51] 2-D slices of 2-chlorothiophene inside large coffin-shaped ZSM-5 crystals were recorded, in which the intensity pattern of these head-to-tail oriented probe molecules revealed the subunit structure of such crystals in detail.[29] Such MFI-type zeolite materials were employed by Seebacher et al. to visualize mesostructures and, hence, crystalline defects[52] and spatial distribution of probe molecules inside these pores.[53] This methodology was further developed to determine and quantify molecular dynamics inside microporous $AlPO_4$-5 crystals and mesoporous M41S thin films. The molecular characteristics (i.e., orientation, wavelength, and intensity of emission) were correlated to the direct environment of the probe molecule.[54] Steaming of zeolites is a common postsynthesis treatment procedure to alter its characteristics, e.g., acidity and diffusion. The diffusion inside the microporous ZSM-5 framework was increased due to the formation of mesopores and,[55] hence, loss of crystallinity,[56] which could also be visualized by the location of large fluorescing dye molecules inside large coffin-shaped ZSM-5 crystals after steam treatment due to the creation of mesopores.[57] Besides this degradation of the crystalline zeolite framework, steaming affects significantly the acidity of Brønsted and Lewis acid sites.[55,56,58–61] Part of the framework aluminum T sites are removed upon steaming and transfer into extra-framework aluminum sites.[59,62]
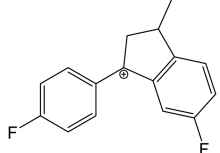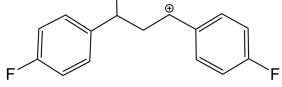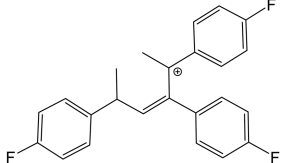
Here we present a systematic confocal polarized fluorescence microscopy investigation of large coffin-shaped ZSM-5. We opted for the fluorostyrene oligomerization reaction as our previous work has indicated that this is a powerful and sensitive reaction for assessing Brønsted acid sites in zeolite-based materials, including zeolite ZSM-5. Table 1 highlights the different carbocations formed, including their spectroscopic fingerprints, as measured by UV–vis[4,6] and synchrotron-based IR[10–12] microspectroscopy, and their possible molecular structures and related dimensions. The confocal fluorescence maps created in this manuscript are to be seen in relation to the recent work of Ristanovic et al.,[15] who provided a detailed μ-XRD investigation on the very same zeolite crystal batches.

The current contribution shows in detail where (i.e., in which zeolite channel and part of the crystal) fluorescent molecules are situated due to their strict orientation inside the channels. The location of these fluorescent molecules could also be distinguished from their fluorescence spectral features. Furthermore, the influence of steaming on the pore architecture of zeolite ZSM-5 and, therefore, the diffusion into the crystal as well as the orientation of the fluorescent molecules is revealed.

2. RESULTS

Three batches of large coffin-shaped ZSM-5 crystals, i.e., parent, steamed at 500 °C, and steamed at 700 °C, were stained with 4-fluorostyrene as a probe molecule. The fluorescence of the oligomerized 4-fluorostyrene formed within the zeolite channels was recorded for 405, 457, 488, 514, 561, and 642 nm laser excitation. The crystals, positioned in both a roof and a gable position, were oriented parallel, 45° (parent and steamed 700 °C), and perpendicular with respect to the polarization plane of the incoming laser light. Hence, the data set consists of 96 z-series, and each of those consist of 18 focal planes, of

Table 1. Spectroscopic Fingerprints of the Reaction Products of the Fluorostyrene Oligomerization for Assessing Brønsted Acid Sites within Zeolite ZSM-5, As Revealed by UV–Vis[4,6] and Synchrotron-Based IR[10−12] Microspectroscopy, Including Their Potential Molecular Structure and Related Dimensions[a]

guest molecule and related molecular structure used for the theoretical calculations	molecular dimensions/Å	UV-vis/ nm	IR/ cm^{-1}
cyclic dimeric carbocation	10 × 6.8 × 3.3	515 (392)	
linear dimeric carbocation	12.7 × 5.6 × 4.7	550 (561)	1534
higher oligomeric carbocation	9.6 × 7.3 × 8.5	606/636 (623)	

[a]The values in parentheses are calculated on the basis of the molecular structures shown. Other molecular structures, including the position of the positive charge and related resonance structures, are possible, and the theoretical spectral transition values provided should only be seen as a trend line, i.e., λ (cyclic dimeric carbocation) < λ (linear dimeric carbocation) < λ (trimeric carbocation), and spectral transitions present in the visible region of the spectrum.

which each focal plane is a summarized image of 32 real fluorescence color images (10 nm × 32 channels). A graphical overview of this approach is given in Figure 2, and details about the instrumentation can be found in Figure S1, Supporting Information.

2.1. Visible Microspectroscopy. Figure 3 shows the absorption spectra and optical images of the parent, steamed 500 °C, and 700 °C ZSM-5 crystals. All stained ZSM-5 crystals showed absorptions at around 550, 515, and one at 580 nm, shifted to longer wavelength (605 and 635 nm). It was previously described in the literature, as summarized in Table 1, that the absorption band at the shortest wavelength belongs to the cyclic dimeric carbocation, whereas the most intense band at 550 nm represents the linear dimeric carbocation.[14,22] Absorption bands at longer wavelength are due to higher oligomers, most probably a trimeric carbocation, as demonstrated in Table 1.[6] In view of the uncertainty of the latter spectral assignment we opted to limit our discussions to the cyclic and dimeric carbocations. After impregnation with 4-fluorostyrene and subsequent temperature treatment, all crystals appeared in a characteristic pink color due to the formed styrene oligomers inside the zeolite pores. The steamed 500 °C crystals appear, in comparison to the other two batches, in a more intense, slightly darker color, as illustrated in Figure 3.

Figure S3, Supporting Information illustrates interference images of the state of the crystals impregnated with 4-fluorostyrene and washed, before the oligomerization was initiated. The four lids, which terminate the ZSM-5 crystal on all four long facets (cf. Figure 1), do not show any noticeable interference, in contrast to the center pyramid reaching out to the crystal tips. In roof position a clear hourglass pattern was observed, which was not the case in gable position. The former statement was confirmed by an image of a (so-called) mixed crystal, in which one-half of the zeolite ZSM-5 crystal was rotated by 90°; hence, there was always a roof and gable tip present at the same time. Here, only this half, which was in a roof position, did show the formerly described hourglass pattern.

2.2. Polarized Fluorescence Confocal Microspectroscopy. In order to assist the reader, we have chosen three sections to present the results, i.e., Orientation and Location of Molecules Trapped in the Zeolite Channels, Spectral Features of Molecules Trapped in the Zeolite Channels, and Influence of Steaming on the Location of Molecules, which are meant to be a guideline. The results may of course not be strictly divided as

Figure 2. Summary of experiments and evaluation principle of the multilaser excitation confocal fluorescence microscopy approach used: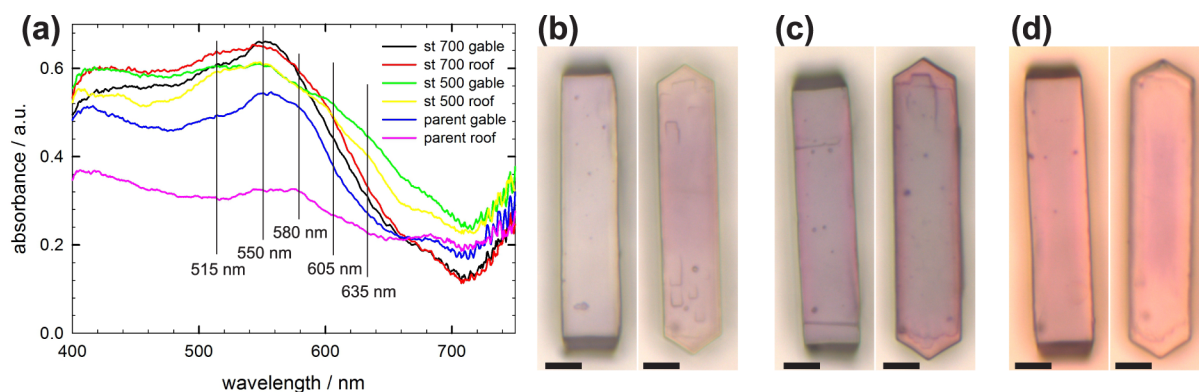 Three sets of large coffin-shaped ZSM-5 samples (parent and steamed at 500 and 700 °C) were stained with 4-fluorostyrene as probe molecule. Both roof and gable positions at 0°, 45° (for parent and steamed 700 °C), and 90° orientation were investigated for their fluorescence during 405, 457, 488, 514, 561, and 642 nm laser excitation. Eighteen focal planes were recorded, each consisting of 32 real color images (i.e., integral intensity of a 10 nm range, 400−720 nm and 430−750 nm, respectively). Hence, the presented data set contains a total of 96 sets of focal planes. Afterward, during data evaluation, 3-D (i.e., depth dependent) spectra were extracted for each set of focal planes from a region of interest.

Figure 3. (a) Absorption spectra of the ZSM-5 crystals; (b) parent, (c) steamed 500 °C, and (d) steamed 700 °C presented as photoimages. Those were the very same crystals investigated in the fluorescence microscopy investigations in this manuscript and obtained after impregnation and reaction of 4-fluorostyrene at 180 °C. Polarization-dependent absorption spectroscopy investigations were presented for parent and steamed 700 °C in Sprung et al.[9] and Figure S4, Supporting Information, respectively. Scale bars represent 10 μm in width.

such, and cross-links to other features occur. The observed polarization plane of emitted fluorescence light was always vertical (i.e., north–south). The whole set of data measured is presented in Figures S7–S42, Supporting Information.

2.2.1. Orientation and Location of Molecules Trapped in the Zeolite Channels. Figure S5, Supporting Information, shows two intergrown ZSM-5 crystals. The cross was oriented as such that for one of the two crystals each roof area of the tip was positioned perpendicular to the recorded polarization plane. Thereby the equality of both sides of the crystal tip was confirmed. Any features, which were observed for crystal orientations other than 0° and 90°, were, therefore, considered to appear in an equal manner at the respective other side of the ZSM-5 crystal (due to symmetry) in case the crystal would be rotated 90° from that (e.g., 45° and −45°).

Figure 4 illustrates crystals in roof and gable orientation of all three ZSM-5 batches. Let us first focus on orientation-related features: Parent ZSM-5 crystals, which were oriented with its long axis parallel to the analyzer position, showed a rim of fluorescence on the outer edge of the crystal. The center part was dark through the whole depth. Rotating the crystal by 90°,
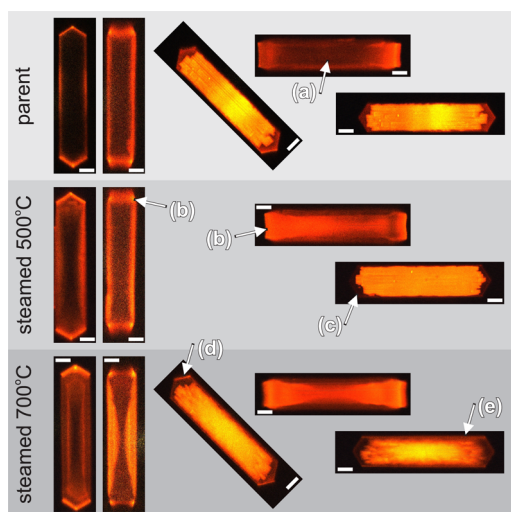
Figure 4. Combined view on orientation and steaming related features of ZSM-5 crystals stained with 4-fluorostyrene: λ_{ex} = 561 nm, highlights a–e are described in the text. Investigated polarization plane is north–south, i.e., vertical. Scale bars represent 10 μm in width.

to be aligned perpendicular to the analyzer position, made the center appear fluorescent. Highlight a in Figure 4 shows a focal plane around the center of the crystal. It is pointed out here that with increasing depth the intensity of emitted light was strongly decreasing.

Intense absorption of excitation light in the upper layers of the crystal significantly reduced the fluorescence intensity inside the crystal. The tip of the crystal viewed in roof position (highlighted as b in Figure 4) was fluorescent in both 0° and 90° orientation, which was most pronounced for excitation frequencies λ_{ex} = 561 nm. In the gable position this inner part of the tip triangle was dark (highlight c). The tip part in the gable position revealed another feature, marked by d. When oriented to 45° with respect to the analyzer position, only one part of the tip was observed. It was confirmed by preliminary experiments that this observation was symmetric and may therefore be translated to the other part of the tip, cf. Figure S5, Supporting Information. The spectral intensities of the same spot in 0° and 45° orientation were similar. In highlight e the edge remains dark when the crystal was in 90° orientation, hence, complementary to the observed fluorescent rim in 0° orientation.

Figure 5 illustrates the complementary information gathered from the presented experiments: When viewed from both directions, an hourglass pattern appeared. In gable position, this was revealed by a large fluorescing area, which shrunk toward the center of the crystal and increased again in deeper layers. Figure 5a nicely illustrates this observation by a high fluorescence intensity at the top and bottom layers compared to the center. In contrast to that, Figure 5b shows high fluorescence intensity all the way down. Viewing the crystal in roof position shows an hourglass pattern as well, however, from the side. The fluorescence intensity in a region between the crystal center and the tip (Figure 5c) remains high all the way through the crystal. In contrast, a region of interest somewhere between the crystal's center and long edge confirms the hourglass pattern with its narrow center; and a high emission intensity was only observed in the top layers (cf. Figure 5e).

2.2.2. Spectral Features of Molecules Trapped in the Zeolite Channels. Figure 6a,b shows the complementary information gathered by observing the crystals' fluorescence in 0° and 90° orientations. In gable orientation the fluorescence of the roof parts of the tips were most intense, in comparison to the long edges, and observed from top to bottom. It can clearly
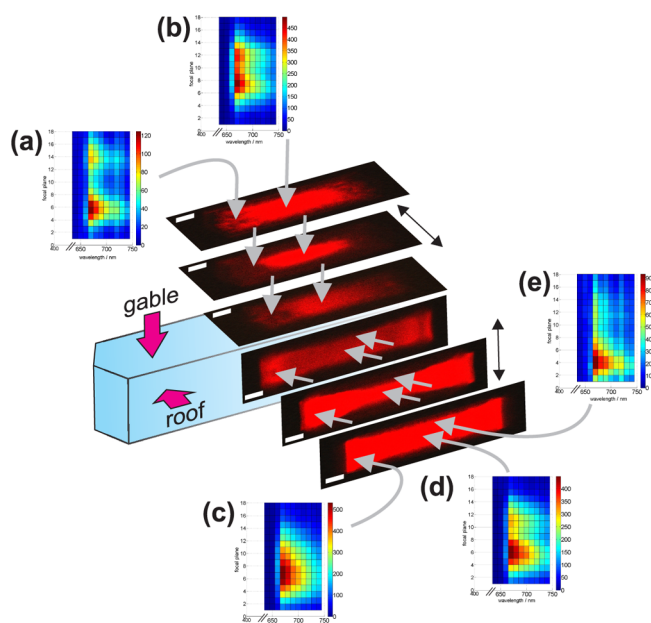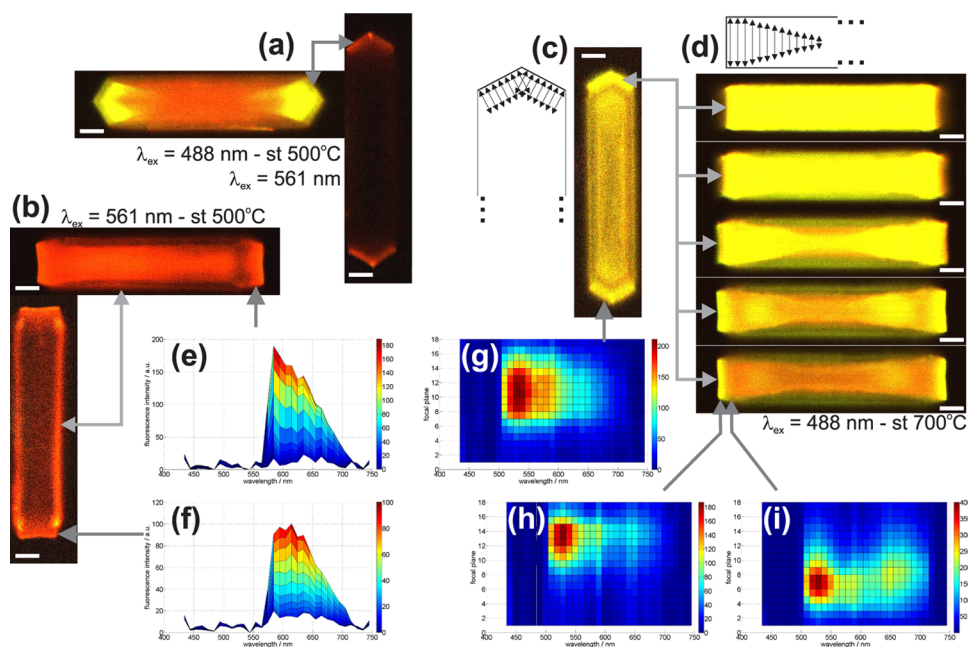
Figure 5. Zeolite ZSM-5 crystal, steamed at 700 °C, viewed in roof and gable orientation, excited with a 642 nm laser. Schematic drawing of the crystal is completed by focal planes of the top, middle, and bottom plane (with respect to the viewing direction). Arrows indicate the area from which depth-dependent spectra were extracted: (a,c) left of center, (b,d) center, and (e) top of center. Double-headed arrows indicate the recorded polarization plane, i.e., perpendicular to the long crystal axis. Scale bars represent 10 μm in width.

strictly oriented. Similar observations for the crystal's long edge in roof position are illustrated in Figure 6b.

The tips were observed to be fluorescent for both 0° and 90° orientation. For a comprehensive overview see also Figures 4d and S5, Supporting Information. The scheme of Figure 6c illustrates the polarization plane of the recorded fluorescence light. The fluorescence spectrum (Figure 6g) expresses the fact that this fluorescence was observed along the whole depth of the crystal. Now, the crystal is rotated in Figure 6c around its long axis; the crystal would now be in roof position, i.e., as in Figure 6b. Fluorescence of the tip was also observed here in 0° orientation. Hence, the channels in the tip part, which was highlighted in Figure 6c, are oriented presumably along the crystal's long axis. This suits the pore structure model of such ZSM-5 crystals, and the latter mentioned observed fluorescence polarization behavior originates from molecules entrapped inside those sinusoidal channels of the tip region.[6] Another conclusion may be drawn by comparing Figure 6c and 6d. In both orientations, the outer part of the tip appeared fluorescent. Thus, the fluorescence light was polarized perpendicular to the outer tip surface in the gable orientation and additionally parallel to the crystal's short axis. Due to the strict orientation behavior of the recorded fluorescence light, it could be speculated whether these two spectral features originated from the same molecule. The crystallographic model of the ZSM-5 crystal, illustrated in Figure 1, contains straight and sinusoidal channels. Following this model, the fluorescence in gable position was originating mainly from molecules aligned inside the sinusoidal channels. Fluorescence (of the crystal tip) in roof position was then emitted by molecules inside straight pores. Spectra extracted from those regions reveal features which substantiate the formerly proposed statement: All three spectra in Figure 6g–i show a band at 530/540 nm. In Figure 6g, however, appeared an additional band at 580 nm, which was missing in both spectra taken in roof position (Figure 6h,i).

be seen in Figure 6a how narrow this fluorescing volume was. Exactly this aforementioned volume did not appear (fluorescent) when the crystal was turned to the 90° orientation. Hence, the molecules aligned within the zeolite channels were

Figure 6. (a,b) Location: the rim, which is fluorescent in the vertical crystal, is not fluorescent in the horizontal one. (a) Zeolite ZSM-5 crystal was steamed at 500 °C and excited at 488 and 561 nm in horizontal and vertical orientations, respectively. (c,d) Spectral features: crystals were steamed at 700 °C and excited at 488 nm; the schematic drawings highlight the polarization plane of recorded fluorescence light. (e–i) Fluorescence spectra extracted from the indicated positions. Scale bars represent 10 μm in width.
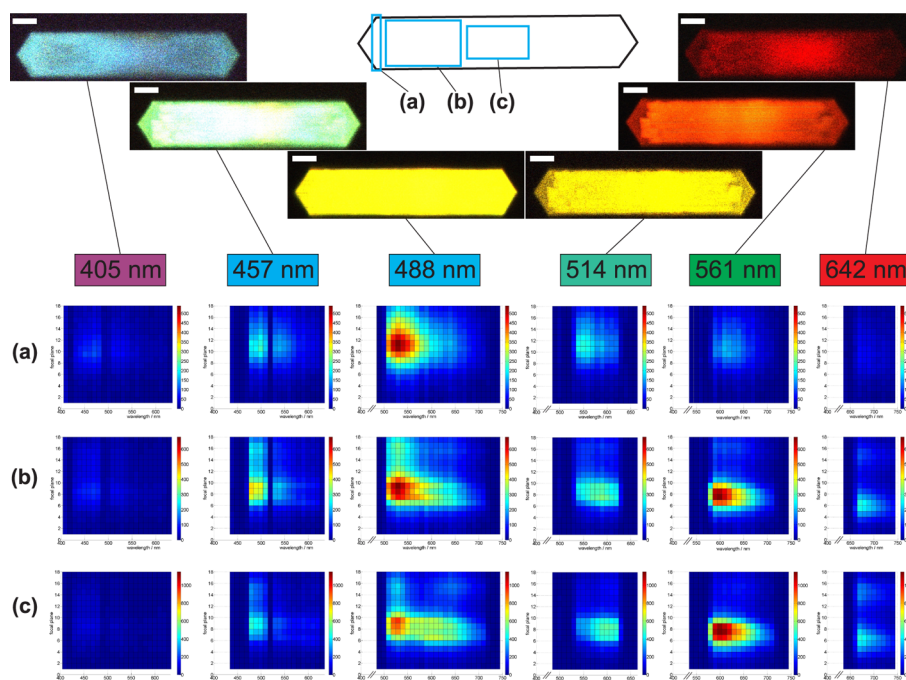
Figure 7. Parent zeolite ZSM-5 crystals in gable position and 90° oriented. Focal planes from the center of the crystal. Depth-dependent fluorescence spectra were extracted from (a) the tip, (b) body between tip and center, and (c) center region. Scale bars represent 10 μm in width.

Such a spectral difference was also observed between the very same region investigated in 0° and 90° orientation, as illustrated in Figure 6e,f. In Figure 6f the fluorescence at longer wavelength (i.e., 610−620 nm) was more intense than in Figure 6e. In summary, a longer wavelength fluorescence occurred in 0° orientation in comparison to 90° orientation. Furthermore, comparing the spectra in Figure 6g and 6h highlights the depth sensitivity of the spectral features. The band at 530 nm was observed for the whole crystal depth of just part of it, respectively, according to the crystals' shape.

Figure 7 provides a comprehensive overview of depth-dependent spectra extracted from three regions (i.e., tip, between tip and center, and center of the crystal) of a parent crystal in 0° orientation and gable position. All extracted spectra were scaled with respect to the most intense fluorescence band in the region of interest among all excitation lines. Fluorescence upon 405 nm excitation was in all cases very low. The highest emission intensity was observed for 488 nm excitation in Figure 7a, whereas it was more intense for 561 nm excitation in Figure 7c. This corresponds to the observed absorption bands reported in the section on visible microspectroscopy. A bathochromic shift in the overall fluorescence intensity was observed toward the crystal's center (i.e., from Figure 7a to 7c). This is most clearly seen for the shift of the fluorescence band for 514 nm excitation. The most intense emission for 457 nm excitation was observed in region b (between center and tip). The fluorescence remained low in the other two regions. In Figure 7a an intense emission was observed for 488 nm excitation at 530 nm; those for 514, 561, and 642 nm were low in intensity. Toward the center of the crystal, a second band appeared at 590 nm. The fluorescence band for 514 nm excitation shifts from 550 nm at the tip to 590 and 600 nm toward the center of the crystal, respectively. The latter band might have reached out further into the red part of the spectrum. However, the 457/514 dichroic mirror did cut the light for wavelengths greater than 630 nm. An emission band

with high intensity at 600 nm was extracted from the crystal's body (i.e., Figure 7b,c) for 561 nm excitation. It was, however, observed with low intensity at the crystal's tip. The emission characteristic for 642 nm excitation followed those observed for 561 nm excitation, i.e., low/negligible intensity at the tip with increasing emission intensity toward the center of the crystal. Due to the weaker absorption of the 642 nm laser in the upper layers, the fluorescence of the crystal's top and bottom subunit could be observed.

2.2.3. Influence of Steaming on the Location of Molecules. The investigated set of parent ZSM-5 crystals, fully described in the previous section, were additionally steamed at 500 and 700 °C, also called mildly and severely treated in the literature, respectively.[7] An overview is given in Figure 4. Parent crystals (in the upper part of this figure) showed a narrow rim of emission in 0° orientation for both gable and roof position. The center part of the crystal remained largely dark; thus, no emission of this polarization was recorded from that region. Crystals, which were steamed at 500 °C, did show already a significant broadening of the fluorescent rim reaching out into the center. This was even more pronounced for crystals treated at 700 °C in steam. Crystals in roof position did literally show a complementary fluorescence pattern when compared in 0° and 90° orientations. Fluorescent regions appeared dark in the respective other orientation. For steamed crystals at 700 °C, it seems that a kind of a small replicate of the large crystal's shape was observed inside the crystal. This is in line with the subunit model proposed by Karwacki et al.[17] Roeffaers et al. proposed the 3-component model to be preferred for coffin-shaped ZSM-5 crystals.[19] Our results suggest for the samples investigated here the validity of the 2-component model, and Figures S3 and S4 (second crystal on the lower right corner), Supporting Information, provide the basis for this conclusion.

Furthermore, steam treatment apparently decreased the amount of fluorescent molecules in the outer crystal layers. The absorption of excitation light decreases in these regions;

hence, the emission of molecules in deeper layers toward the center could therefore be observed. Crystals in 90° orientation in Figure 4 clearly illustrate this change. The center part remained dark for a parent crystal; however, for a crystal steamed at 700 °C the inner subunit structure could clearly be observed. Such degradation of the zeolite framework and the creation of mesopores were also observed and confirmed by Aramburo et al.[57]

Figure 8 illustrates gable-positioned crystals in 90° orientation as parent and steamed at elevated temperatures
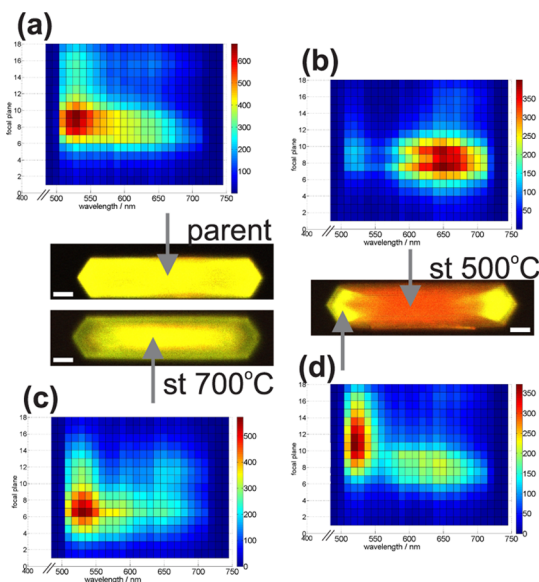
Figure 8. Influence of steaming: ZSM-5 crystals (parent, steamed (st) 500 °C, and steamed (st) 700 °C) in gable position oriented 90° with respect to the analyzer position; excitation wavelength was 488 nm. Depth-dependent fluorescence spectra from (a−c) the center part of the crystal and (d) the yellow tip part. Scale bars represent 10 μm in width.

excited at 488 nm. Parent crystals showed a uniform fluorescence representing the whole crystal shape, which was clearly different from the very same crystal excited at 561 nm (cf. Figure 4). This was only observed for parent crystals. Those crystals, which were treated in steam at 500 and 700 °C, respectively, did not show emission from the tip parts in this orientation. A fluorescence band at 530 nm was observed in Figure 8a and 8c. In the latter, treated at 700 °C in steam, a second band at 650 nm appeared also in deeper layers. A clearly two-divided fluorescence map was recorded for 500 °C steam-treated ZSM-5 crystals. Their tip parts, note without the formerly described rim (cfr. Figure 6a), emitted bright yellow light at 520 nm, whereas the center part emitted orange-red light at around 650 nm.

3. DISCUSSION

3.1. Visible Microspectroscopy. The obtained absorption spectra, shown in Figure 3, are in line with previously reported spectra of oligomerized 4-fluorostyrene inside large zeolite ZSM-5 crystals by Stavitski et al.[6] The crystal batch after mild steaming conditions (i.e., 500 °C) showed a higher absorption at longer wavenumbers, compared to parent crystals, which was also found on zeolite ZSM-5 powder samples.[14] The more intense coloration for mildly compared to parent and severely steamed crystals was confirmed in investigations by Aramburo

et al.,[7] who concluded an increasing and decreasing activity (i.e., reactivity and therefore formation of colored reaction products) with increasing steaming temperature.

3.2. Orientation and Location Related Features. The experiments demonstrate the strict polarization of fluorescence light, originating from molecules entrapped inside the zeolite pore system (cf. Figures 4, 6, and S5, Supporting Information). In the experimental section data recording and treatment it was considered that the transition dipole moment vector is parallel (or at least within 20°) with respect to the long axis of the oligomeric reaction products.[63] Thus, for further interpretation of the results the recorded polarization plane of fluorescence light is parallel to the long axis of an elongated oligomeric species, which is oriented parallel to a channel direction of the zeolite. For clarity, the pore architecture of zeolite ZSM-5, as shown in Figure 1, shall be briefly repeated; straight pores are oriented parallel to the short axis of the crystal for the four pyramidal subunits (which is along [010]), and sinusoidal pores are oriented perpendicular to the straight pores and parallel to [100]. For the closing units, the straight pores are parallel to the rectangular facets and hence open to the triangular facets.[8,15]

A strong fluorescence signal was recorded parallel to [010] for the pyramidal subunits; hence, molecules were oriented along the straight pores in these sections. This was observed and confirmed by UV−vis microscopy.[4] The value added by the results in Figure 4 was the observation of a fluorescent rim, showing emission polarized parallel to the crystal's long axis. Similarly, a rim of absorption light polarized along the long crystal axis, including the tips, was reported by Sprung et al.,[9] employing differently polarized light for UV−vis absorption microscopy (in this reference Figure 1, note the different orientation of the polarizer and analyzer, respectively, cf. the images labeled with 0°). Also, Roeffaers et al.[31,32] observed a fluorescent rim during furfuryl condensation. Their conclusion (by EBSD[31]) and ours for this observation was/is that this fluorescence was originating from molecules inside the sinusoidal channels.

In connection to the last argument in the former paragraph, why did this observed fluorescent rim not originate from randomly oriented species on the zeolite surface? First, a rinsing step was performed before inducing the reaction by a temperature increase to minimize/exclude such reaction at the outer crystal surface. Second, crystals in gable position and 90° orientation did not show any fluorescence of the tip region (cf. Figure 4). In a more focused manner, this is presented in Figure S5, Supporting Information. Hence, this fluorescence light was strictly polarized and, thus, originated from molecules inside the zeolite pores. Sinusoidal pores open into the {100} faces, however, not perpendicular (in that case no fluorescence would have been observed). For the tip region, it is suggested, based on the observations made in Figures S5, Supporting Information, and 6c, that the sinusoidal pores are open perpendicular to the roof areas of the tip. Following the observations made in Figure 4 for parent and steamed samples, it can be speculated whether this observed fluorescent rim is an intrinsic characteristic of the diffusion and reactivity of such a ZSM-5 crystal. It might also be considered that this was already the sign of a degrading pore architecture/mesopore creation due to postsynthesis treatment (e.g., calcination). After steam treatment a clear increase of this fluorescent rim was observed toward the center of the crystal. The outer layers of the crystals seem to decrease in crystallinity; the absorption of excitation

light was much lower for mildly and severely steamed crystals, i.e., fluorescence of center parts of the crystal could be recorded (cf. Figure 4). This aspect was also observed for visible absorption microscopy, shown in Figure S4, Supporting Information.

Another question, which might arise in connection with Figure 4 and the illustration of parent crystals in the upper part is why has no fluorescence been observed from probe molecules inside sinusoidal channels from the bulk of the crystal, hence, from the intact framework? Sinusoidal channels are open to the majority of the outer surface of such ZSM-5 crystals and were therefore at first in contact with the liquid 4-fluorostyrene. It is assumed that both sinusoidal and straight channels were filled with monomeric 4-fluorostyrene molecules before their oligomerization was initiated, as illustrated schematically by Kox et al.[4] (cf. Figure 4 in that reference). Two major products were assumed to be present after oligomerization, i.e., a cyclic and a linear dimeric carbocation.[22] Both dimeric carbocations have been placed inside the zeolite channels (cf. Figure 1) according to their steric demands. Cyclic dimers are therefore only expected to be formed at zeolite ZSM-5 channel intersections or defect sites/defected pores in the crystal, where enough room is provided for this molecule. In view of their molecular dimensions and shape we assume that this idea also applies for the trimeric carbocations, as illustrated in Figure 1. In contrast, linear dimeric carbocations are assumed along straight channels only, due to the fact that such a dimer is determined longer (with a length of 14.3 Å)[4] than the dimensions of sinusoidal channels, which are only 12 Å in length (center to center straight channel). Hence, an intact and defect-free framework (no postsynthesis steam treatment) may exclusively incorporate linear dimeric carbocations inside straight channels, whereas cyclic dimeric carbocations are formed at channel intersections due to their steric demands.

3.3. Spectral Features. The visible spectra in Figure 3 report the highest absorption for 550 nm, followed by 580 and 515 nm. Highest fluorescence intensity was observed for the excitation lines 488 and 561 nm. Thus, there was only a clear assignment for a corresponding absorption band for the latter. All other observed emission intensities for the remaining excitation lines remain roughly below half-maximum intensity (cf. Figure 7). Their emission intensity may be explained by the overlap of an excitation line with the remainder of a broad absorption band. Unlike all other excitation lines, these ramps and terraces on the (010) face of the pyramidal subunits for parent crystals were not observed for 488 nm excitation (cf. fluorescence images in Figure 7). Only a uniform, featureless yellow fluorescence appeared. An absorption band for the 488 nm laser line is, however, missing. It might be speculated whether its origin is to be found in a double-excitation process of a UV band (which exists in the suspected wavelength range[64]).

Due to the methodology of applying depth-dependent fluorescence spectra, local spectral features were revealed. In the section Orientation and Location of Molecules Trapped in the Zeolite Channels the location of molecules was discussed and concluded. Molecules in the outer tip region were aligned inside sinusoidal pores, whereas in the bulk part of the tip they were inside straight pores (cf. Figure 6b,d). Fluorescence spectra extracted from these regions, in which molecules inside sinusoidal pores were observed, revealed a shoulder which was 20 and 40 nm shifted compared to the spectra of molecules in

straight pores, for 561 and 488 nm excitation, respectively. Within this content, it is important to compare the spectral features in Figure 6e, 6f, and 6g–i. The straight pores are slightly wider in dimension in comparison to the sinusoidal pores. If the same molecular species is situated inside straight and sinusoidal pores, however, with a different steric environment, that constrains the molecule and therefore shifts the emission band.

Steaming had a highly significant influence on the fluorescence spectra for 488 nm excitation (cf. Figure 8). Upon steaming at 500 °C a red emission around 650 nm appeared in the center of the crystal bulk, whereas the closing subunits on either long end remained bright yellow (around 530 nm). This red fluorescence was observed with much less intensity for severely steamed crystals. Steaming of zeolites changes their diffusion properties and reactivity. A volcano-like behavior could therefore be proposed for the recorded wavelength of fluorescence light, which can be related to the molecule itself, or the interaction of the same molecule with different channel environments. These observations were related to Brønsted acid strength of the samples.[56,58–61] Beyerlein et al. explained an enhanced activity after mild steaming by a synergism between nonframework sites and framework Brønsted sites rather than an increase of the acidity of hydroxyl groups.[65] Aramburo et al.[7] reported this volcano trend for the very same samples by vis microspectroscopy investigations. The observed spectral feature in Figure 8 is, therefore, considered to be related to the Brønsted acid strength inside the zeolite pores. The interaction of the acid site with the oligomeric species may, thus, cause the spectral shift into the red region.

"Which molecule is where?" was the question proposed in the title. Two molecular species (i.e., the cyclic and linear dimeric cations) are in focus. Their different UV–vis absorption bands[4,6] allowed us to visualize selectively one or the other species by choosing the appropriate laser excitation frequency. Hence, fluorescence observed for 488 nm excitation is associated with the location of the cyclic dimeric carbocation species (cf. Figures S19–S24, Supporting Information). Thus, the linear dimeric carbocation species appears fluorescent after 561 nm excitation (cf. Figures S31–S36, Supporting Information). This is a great potential of the employed multilaser excitation confocal fluorescence microscopy approach. Table 2 summarizes the observed locations of both

Table 2. Summary of the Observed Locations of Cyclic and Linear Dimeric Carbocations inside the Channel Architecture of Large Coffin-Shaped Zeolite ZSM-5 Crystals[a]

dimeric carbocation	straight	sinusoidal	intersection	sinusoidal rim	close to surface
cyclic	−	−	×	×	×
linear	×	− (×)	−	×	−

[a]The different locations were either occupied, ×, or not occupied, −. Symbol in parentheses refers to observations at higher temperatures.

product oligomeric species. Due to the steric demands of the cyclic dimeric carbocation species their location is linked to channel intersections. Linear dimeric carbocation species were mainly located in straight channels, however close to the surface (i.e., the rim), and at postsynthesis treated crystals those species also occupy sinusoidal channels. The fluorescence spectra of

molecules inside sinusoidal channels revealed a band/shoulder at longer wavelength compared to the spectra of the same species inside straight channels (in the same region). This distinction was possible only due to the strict alignment of the crystals under the microscope.

4. CONCLUSIONS

The introduction of chemical imaging methods has resulted in a wealth of fundamental information on the interplay between guest molecules and porous host materials, including zeolites.[21,37,46,66−68] In this work, a systematic polarized fluorescence confocal microscopy investigation was presented of three sets of zeolite ZSM-5 crystals (i.e., parent, steamed 500 °C, and 700 °C). Fluorescence spectra were recorded with a spectral range of 320 nm and a spectral resolution of 10 nm for 405, 457, 488, 514, 561, and 642 nm laser excitation and translated into the third dimension. Structural features were determined visually (by inspecting the focal planes and its polarization dependent fluorescence) and spectroscopically (by 3-D fluorescence spectra, distinguishing chemical species). The orientation of elongated fluorescent molecules was recorded on a micrometer scale and linked to the pore architecture of the zeolite.

On the basis of this innovative characterization approach we can make the following conclusions on the 3-D host−guest chemistry of the linear and cyclic dimeric fluorostyrene carbocations, shown in Figure 1 and Table 1, within the zeolite ZSM-5 framework.

(1) In parent ZSM-5 crystals a large portion of the molecules were situated inside the straight pores along the [010] crystal direction, which accommodate exclusively the linear dimeric carbocations.

(2) In parent ZSM-5 crystals it was possible to visualize (and proof) fluorescence originating from the sinusoidal channels as well, which was located in a rim around the crystal. These sinusoidal pores were oriented perpendicular to the rectangular tip surface.

(3) This rim was the onset of pore structure degradation, which was (already) observed for parent crystals (template removal procedure) and increased upon increasing postsynthesis steaming temperature. Hence, more linear dimeric carbocation molecules were observed in sinusoidal channels inside the zeolite crystals toward the center of the crystal, and their increased presence can be regarded as a handy spectroscopic marker for zeolite ZSM-5 degradation. In other words, the developed approach could be used for quality control purposes of freshly prepared zeolite ZSM-5 crystals.

(4) The location of molecules could in addition to its orientation be distinguished by their spectral features. Cyclic and linear dimeric carbocations inside the sinusoidal pores showed an additional fluorescence band shifted to longer wavelength by 40 and 20 nm (for 561 and 488 nm excitation), respectively, compared to the same dimeric carbocations inside the straight pores.

(5) Postsynthesis steaming of zeolite ZSM-5 revealed a volcano-type behavior of the recorded fluorescence, suggesting an optimal steaming temperature for a significantly altered interaction between the zeolite material and the staining molecule used for assessing the location of the Brønsted acid sites.

Although a specific type of zeolite framework structure (i.e., MFI) was employed in this work, the presented methodology is transferable to other types of zeolite framework structures (e.g., FAU and MOR) in which linear dimeric and cyclic dimeric fluorostyrene species can reside. Furthermore, one may envisage other scientific endeavors in which optical and spectral resolutions, molecular location, and orientation of guest molecules in the third dimension may be of great interest. The multilaser excitation confocal fluorescence microscopy toolbox has now been developed to make such detailed studies possible.

5. EXPERIMENTAL SECTION

5.1. Materials and Methods. Large ZSM-5 crystals (20 × 20 × 100 μm) were provided by ExxonMobil and used in its acid form. The samples were placed on a borosilicate glass in an open Linkam cell (FTIR 600, Linkam Scientific Instruments). At a temperature of 30 °C, the samples were impregnated with an excess of 4-fluorostyrene (99%, Sigma-Aldrich, used as received). After the reactant had evaporated the sample was rinsed twice with mesitylene (97%, Sigma-Aldrich, used as received) for cleaning purposes. Since it can be expected that mesitylene does not diffuse into the pores of ZSM-5, only excess reactant (fluorostyrene) from the outside of the crystals was assumed to be rinsed off during this procedure. The reaction was initiated by increasing the temperature rapidly to 180 °C, at which it was kept during all investigations.

5.2. Instruments. An upright optical microscope from Olympus (BX 41) was employed in reflectance mode, equipped with a 50× 0.5 NA dry objective and a 30 W halogen lamp. Incoming light was plane polarized in the E−W plane (i.e., east−west, horizontally oriented) through an U-PO3 polarizer from Olympus. Reflected light was recorded with a CCD video camera (ColorView IIIu, Soft Imaging System GmbH) and observed through a 50/50 double view-port tube. The reflected light was analyzed with a rotatable analyzer U-AN360 from Olympus. This device was completed by an angular scale to increase the precision of adjusting its orientation. The sample was oriented manually under the objective to positions of 15° steps, and the analyzer position was adjusted to steps of 30° with respect to the polarization plane of incoming light. Hence, at each crystal orientation (0°, 15°, 30°, ..., 165°) six analyzer positions (0°, 30°, 60°, ..., 150°) were recorded. Fluorescence microscopic investigations were performed with a Nikon ECLIPS 90i confocal microscope in reflectance mode; its essential optical parts are illustrated in Figure S1, Supporting Information. Excitation light was provided by an ensemble of four laser heads, of which one was tunable in its output frequency; thus, laser light of 405, 457, 488, 514, 561, and 642 nm was employed. Laser light passed the polarizer inside the instrument after the dichroic mirror (DM) and before it was focused through a 100× 0.73 NA dry lens on the sample. Thus, the emission light did pass the same polarizer before the dichroic mirror on the way to the analyzing unit. The polarization plane of excitation/emission light was, therefore, the same, i.e., N−S (i.e., north−south, vertically oriented). Optical multimode fibers carried excitation light and fluorescence light from the sources to the microscope and to the spectral analyzer, respectively. The microscope was equipped with a Nikon A1 scan head, which accommodated the optics to couple fiber optics for excitation and emission light with the microscope, and the dichroic mirrors. An overview on the dichroic mirrors employed is given in Table 3.

A Linkam cell (FTIR 600, Linkam Scientific Instruments) was mounted on the sample stage of the microscopes to supply heat. An in-house made rotatable sample holder (stainless steel) was employed to orient the sample with respect to the incoming light polarization plane.

5.3. Data Recording and Treatment. *Recording Specifications.* The spectral analyzer in the Nikon A1 system was equipped with 32 photomultiplier tubes (PMTs) to collect the emission light in the 400−720 nm (for ν_{ex} = 405 nm) and 430−750 nm (all other laser

**Table 3. Overview of the Dichroic Mirrors Employed during the Experiments**

laser line/ nm	pin hole size/μm	dichroic mirror	supplementary information
405	92.4	405/488	transmission <630 nm
457	103.0	457/514	transmission <630 nm
488	110.3	405/488	transmission <630 nm
488	110.3	405/488/561	
514	114.6	457/514	transmission <630 nm
561	125.7	405/488/561	
642	142.4	405/488/561/642	

lines) range with a resolution of 10 nm. The sample (large ZSM-5 crystals) was oriented with its long axis parallel, at 45°, and perpendicular with respect to the polarization plane of incoming laser light. A z-series of 18 focal planes was taken for each orientation and laser line with a step size of 1.2 μm. Thus, every z-series contained 18 × 32 images of 512 × 128 pix^2, with a pixel size of 0.22 μm and a pixel dwell of 57.2 μs. Before exporting the images they were adjusted for brightness according to the optimal conditions of the brightest image of that z-series by the instrument software (Nikon Elements AR). For clarification of terms a z-series consisted of 18 focal planes, and each focal plane is a sum of 32 images, which represent the intensity of light in a 10 nm range.

The narrow pore channels of ZSM-5 contain (in comparison to that) rather large styrene derivate molecules and its oligomeric condensation products. Therefore, a strict anisotropic behavior is expected and considered for the polarization-dependent experiments described here.[28,43,69] The angle between absorption and emission axis was assumed to be <20°, as found by investigations for similar molecules.[63] This was confirmed in preliminary experiments for the oligomeric reaction products investigated here. We consider, therefore, that the elongated reaction products of styrene derivate condensation have their transition dipole moment vectors aligned along the long axis of the molecule for both adsorption and emission. Correction for laser

reflection: Spectra of reflected laser light (observed for laser lines >457 nm) are illustrated in Figure 9, which show the reflections at shorter and longer wavelength with respect to the dichroic mirror position. The laser light was efficiently blocked by this device. The reflection at lower wavelength was found to be a useful benchmark; it is unaffected during the investigations, since fluorescence light does appear at longer wavelength with respect to the excitation frequency (for single-excitation processes). It was, therefore, possible to correct all images (for excitation with 488, 514, 561, and 642 nm laser light) for their laser reflection. Both reflection spectra in a bare crystal and the sample holder were fairly similar; however, the reflection spectra in the crystal were eventually used for correction. Figure 9c−e illustrate the result of the following procedure, exemplified for three images for 514, 561, and 642 nm excitation. For every focal plane, the image of the channel, which represents the maximum intensity of the laser reflection at lower wavelength, with respect to the dichroic mirror, was taken as benchmark. The intensity of the pixels in these benchmark images were then multiplied by the value of the relative intensity of the laser reflection spectrum of a specific wavelength range (cf. spectra in Figure 9). The resulting intensity values were then subtracted from the pixel intensities of the respective channel. (For example, ν_{ex} = 488 nm, i.e., benchmark for subtraction is channel 5, image to correct is channel 4. Pixels of the image from channel 5 are multiplied with the value of channel 4 in the reflection spectrum (cf. Figure 9). The resulting pixel intensities are subtracted from the raw data image of channel 4.)

Dichroic Mirror Characteristics. The dichroic mirrors 405/488 and 457/514 did transmit light with a wavelength <630 nm. This cuts a large portion of the fluorescence light in the red region, illustrated in Figure 10a,d. This drawback could, at least for 488 nm excitation, be circumvented by recording the same z-series twice with the 405/488 and 405/488/561 dichroic mirror inserted, respectively. The latter dichroic mirror, obviously, does not transmit light in a narrow region around 561 nm, which is clearly illustrated in Figure 10b,e. Thus, images of channels <600 nm and 600 nm were combined (cf. Figure 10c and 10f) and represent from now on the data set taken at 488 nm excitation.
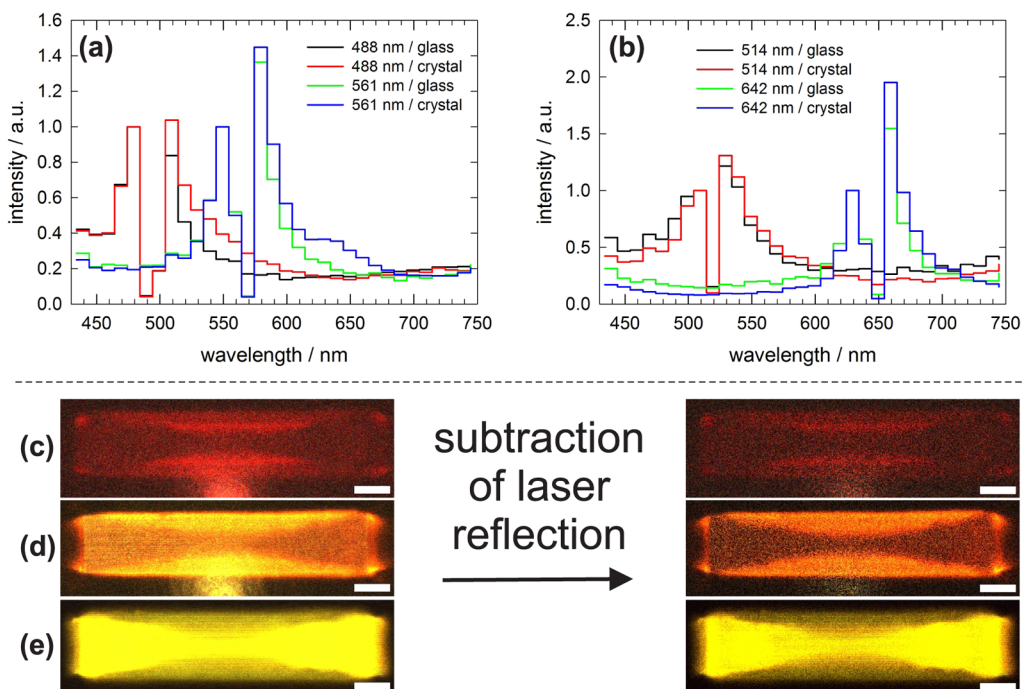
Figure 9. (a,b) Laser reflection spectra for 488, 514, 561, and 642 nm laser lines, recorded on a glass sample holder and on bare ZSM-5 crystal. Subtraction of laser reflection for (c) 642, (d) 561, and (e) 514 nm laser light at steamed 700 °C ZSM-5 crystals. The spot beneath the crystals of the images in the left column was originating from the laser reflected in the sample holder. The signal of this reflection was effectively subtracted from the images by the procedure described in the text (compare images in the left and right columns). Scale bars represent 10 μm in width.
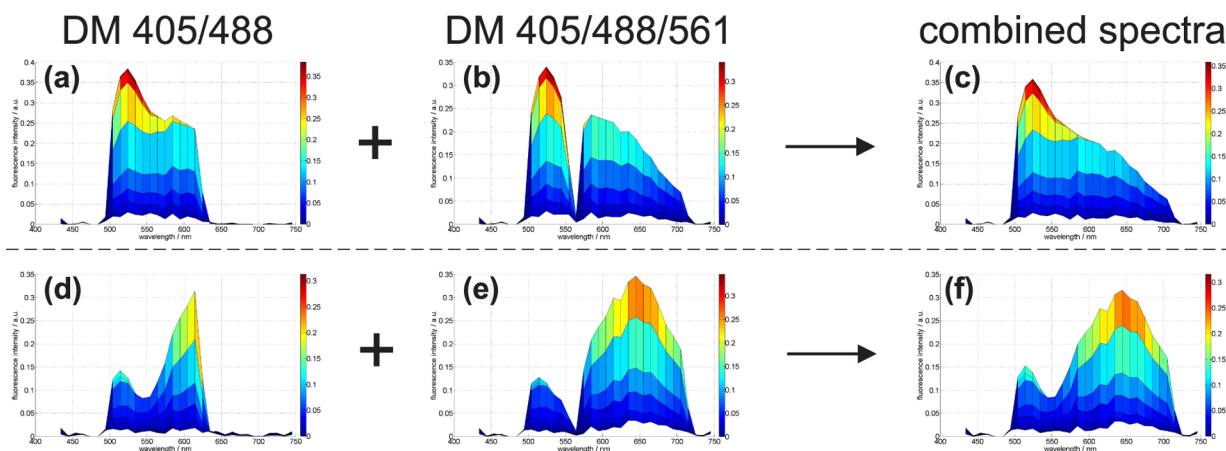
Figure 10. Transmission of fluorescence light of dichroic mirrors and 488 nm excitation: (a−c) parent and (d−f) steamed 500 °C ZSM-5 crystal, spectra extracted for (a,d) dichroic mirror 405/488 and (b,e) dichroic mirror 405/488/561. (c,f) Combined values of the former two.

Semiquantification. All spectra were recorded with optimal optical conditions, i.e., laser intensity, detector gain, and image brightness. An at least semiquantitative description of the achieved fluorescence signals was, however, desirable. Therefore, a normalization procedure was applied as follows: A square of 10×10 pix^2 was defined in every focal plane outside the crystal, picking up the image/background noise caused by the detector gain. The average intensity value of these 100 pixel was additionally averaged over all 18 focal planes in this z-series. Figure S2a, Supporting Information, illustrates these values after 10 repetitions and their standard deviation. For further data processing, the average noise was then normalized by the number of pixels (i.e., 100). Hence, each z-series was assigned a noise-intensity per pix^2 value, which was utilized to semiquantify all fluorescence spectra. Figure S2b−d, Supporting Information, shows focal planes of a steamed 700 °C ZSM-5 crystal for 488, 514, and 561 nm excitation. Their fluorescence spectra, extracted from the whole crystal without the tips, in Figure S2e, Supporting Information, were not normalized and represent an average of the intensities in that region of interest. Normalized fluorescence spectra (Figure S2f, Supporting Information) show a different order of intensities among the three excitation lines compared to uncorrected spectra.

Summary of Experimental Results and Evaluation Principle. A large part of the Results and Discussion sections consists of 3-D spectra, which represent depth-dependent fluorescence spectra of a region of interest (ROI); Figure 2 illustrates this principle. Such a ROI, a rectangle, was freely adjusted to the size of the area of interest in the images. The values for each channel in that ROI were then summed up and divided by its size in pix^2. Finally, the spectra were normalized with respect to the assigned noise-intensity per pix^2 value. All data treatment described in this section has been carried out with homemade MatLab scripts (MatLab R2009a). Image processing was (in most cases) carried out in the hsv-color space in which the third matrix represents the pixel intensity. The whole data set including the commented MatLab script to extract 3-D fluorescence spectra is available in the Supporting Information.

5.4. Theoretical Calculations. The theoretical approach was applied previously to gain insight into the thiophene oligomerization products formed on zeolite ZSM-5-containing extrudates.[70] The optimized geometry for each compound was obtained using the hybrid meta GGA density functional M06-2X[71] with the 6-31+G(d,p) standard basis set. All harmonic vibrational frequencies were real; therefore, the structures were minima on the potential energy surface. Time-dependent (TD) DFT excited states calculations were carried out at M06-2X/6-31+G(d,p) level. All calculations were performed using Gaussian 09.[72]

CLARIFICATION

All images, which appear from the Results section on, are oriented as they were recorded, i.e., the incoming light polarization for visible microscopy is E−W (i.e., parallel to the short axis of the sheet of paper), and for fluorescence microscopy it is N−S (i.e., parallel to the long axis of the sheet of paper). The short axis of all fluorescence images represents 28.2 μm, and scale bars represent 10 μm in width.

ASSOCIATED CONTENT

⑤ Supporting Information

Additional information concerning data treatment, visible microspectroscopy, and fluorescence microscopy, showing all polarization-dependent fluorescence images of this work. This material is available free of charge via the Internet at http://pubs.acs.org.

AUTHOR INFORMATION

Corresponding Author

*b.m.weckhuysen@uu.nl

Notes

The authors declare no competing financial interest.

REFERENCES

(1) Ertl, G.; Knozinger, H.; Weitkamp, J. *Handbook of Heterogeneous Catalysis*; VCH-Wiley: Weinheim, 1997; Vol. I, p18.

(2) Hagen, J. *Technische Katalyse*; VCH-Wiley: Weinheim, 1996; p 243.

(3) Jimenez-García, G.; Aguilar-Loppez, R.; Maya-Yescas, R. *Fuel* **2011**, *90*, 3531.

(4) Kox, M. H. F.; Stavitski, E.; Weckhuysen, B. M. *Angew. Chem., Int. Ed.* **2007**, *46*, 3652.

(5) Lu, J.; Roeffaers, M. B. J.; Bartholomeeusen, E.; Sels, B. F.; Schryvers, D. *Microsc. Microanal.* **2014**, *20*, 42.

(6) Stavitski, E.; Kox, M. H. F.; Weckhuysen, B. M. *Chem.—Eur. J.* **2007**, *13*, 7057.

(7) Aramburo, L. R.; Karwacki, L.; Cubillas, P.; Asahina, S.; de Winter, D. A. M.; Drury, M. R.; Buurmans, I. L. C.; Stavitski, E.; Mores, D.; Daturi, M.; Bazin, P.; Dumas, P.; Thibault-Starzyk, F.; Post, J. A.; Anderson, M. W.; Terasaki, O.; Weckhuysen, B. M. *Chem.—Eur. J.* **2011**, *17*, 13773.

(8) Agger, J. R.; Hanif, N.; Cundy, C. S.; Wade, A. P.; Dennison, S.; Rawlinson, P. A.; Anderson, M. W. *J. Am. Chem. Soc.* **2003**, *125*, 830.

(9) Sprung, C.; Weckhuysen, B. M. *Chem.—Eur. J.* **2014**, *20*, 3667.

(10) Stavitski, E.; Pidko, E. A.; Kox, M. H. F.; Hensen, E. J. M.; van Santen, R. A.; Weckhuysen, B. M. *Chem.—Eur. J.* **2010**, *16*, 9340.

(11) Stavitski, E.; Kox, M. H. F.; Stewart, I.; de Groot, F. M. F.; Weckhuysen, B. M. *Angew. Chem., Int. Ed.* **2008**, *47*, 3543.

(12) Stavitski, E.; Kox, M. H. F.; Weckhuysen, B. M. *Stud. Surf. Sci. Catal.* **2008**, *174A*, 21.

(13) Karwacki, L.; Weckhuysen, B. M. *Phys. Chem. Chem. Phys.* **2011**, *13*, 3681.

(14) Aramburo, L. R.; Wirick, S.; Miedema, P. S.; Buurmans, I. L. C.; de Groot, M. F.; Weckhuysen, B. M. *Phys. Chem. Chem. Phys.* **2012**, *14*, 6967.

(15) Ristanovic, Z.; Hofmann, J. P.; Deka, U.; Schulli, T. U.; Rohnke, M.; Beale, A. M.; Weckhuysen, B. M. *Angew. Chem., Int. Ed.* **2013**, *52*, 13382.

(16) Weidenthaler, C.; Fischer, R. X.; Shannon, R. D. *J. Phys. Chem.* **1994**, *98*, 12687.

(17) Karwacki, L.; Kox, M. H. F.; de Winter, D. A. M.; Drury, M. R.; Meeldijk, J. D.; Stavitski, E.; Schmidt, W.; Mertens, M.; Cubillas, P.; John, N.; Chan, A.; Kahn, N.; Bare, S. R.; Anderson, M.; Kornatowski, J.; Weckhuysen, B. M. *Nat. Mater.* **2009**, *8*, 959.

(18) Stavitski, E.; Drury, M. R.; de Winter, D. A. M.; Kox, M. H. F.; Weckhuysen, B. M. *Angew. Chem., Int. Ed.* **2008**, *47*, 5637.

(19) Roeffaers, M. B. J.; Ameloot, R.; Baruah, M.; Uji-i, H.; Bulut, M.; De Cremer, G.; Müller, U.; Jacobs, P. A.; Hofkens, J.; Sels, B. F.; De Vos, D. E. *J. Am. Chem. Soc.* **2008**, *130*, 5763.

(20) Pollack, S. S.; Sprecher, A. F.; Frommell, E. A. *J. Mol. Catal.* **1991**, *66*, 195.

(21) Kerssens, M. M.; Sprung, C.; Whiting, G. T.; Weckhuysen, B. M. *Microporous Mesoporous Mater.* **2014**, *189*, 136.

(22) Corma, A.; Garcia, H. *J. Chem. Soc., Dalton Trans.* **2000**, 1381.

(23) Buurmans, I. L. C.; Pidko, E. A.; de Groot, M. J.; Stavitski, E.; van Santen, R. A.; Weckhuysen, B. M. *Phys. Chem. Chem. Phys.* **2010**, *12*, 7032.

(24) IZA Structure Commission, http://www.iza-structure.org/databases/.

(25) Olson, D. H.; Kokotailo, G. T.; Lawton, S. L.; Meier, W. M. *J. Phys. Chem.* **1981**, *85*, 2238.

(26) Caro, J.; Noack, M.; Richter-Mendau, J.; Marlow, F.; Petersohn, D.; Griepentrog, M.; Kornatowski, J. *J. Phys. Chem.* **1993**, *97*, 13685.

(27) Kärger, J.; Binder, T.; Chmelik, C.; Hibbe, F.; Krautscheid, H.; Krishna, R.; Weitkamp, J. *Nat. Mater.* **2014**, *13*, 333.

(28) Hoffmann, K.; Marlow, F.; Caro, J. *Zeolites* **1996**, *16*, 281.

(29) Domke, K. F.; Day, J. P. R.; Rago, G.; Riemer, T. A.; Kox, M. H. F.; Weckhuysen, B. M.; Bonn, M. *Angew. Chem., Int. Ed.* **2012**, *51*, 1343.

(30) Day, J. P. R.; Domke, K. F.; Rago, G.; Kano, H.; Hamaguchi, H.; Vartiainen, E. M.; Bonn, M. *J. Phys. Chem. B* **2011**, *115*, 7713.

(31) Roeffaers, M. B. J.; Ameloot, R.; Bons, A.-J.; Mortier, W.; Cremer, G.; de Kloe, R.; Hofkens, J.; De Vos, D. E.; Sels, B. F. *J. Am. Chem. Soc.* **2008**, *130*, 13516.

(32) Roeffaers, M. B. J.; Sels, B. F.; Uji-i, H.; Blanpain, B.; L'hoest, P.; Jacobs, P. A.; De Schryver, F. C.; Hofkens, J.; De Vos, D. E. *Angew. Chem., Int. Ed.* **2007**, *46*, 1706.

(33) Gasecka, A.; Han, T.-J.; Favard, C.; Cho, B. R.; Brasselet, S. *Biophys. J.* **2009**, *97*, 2854.

(34) Brasselet, S. *Adv. Opt. Photonics* **2011**, *3*, 205.

(35) Lavrentovich, O. D. *Pramana* **2003**, *61*, 373.

(36) Jameson, D. M.; Ross, J. A. *Chem. Rev.* **2010**, *110*, 2685.

(37) Janssen, K. P. F.; De Cremer, G.; Neely, R. K.; Kubarev, A. V.; van Loon, J.; Martens, J. A.; De Vos, D. E.; Roeffaers, M. B. J.; Hofkens, J. *Chem. Soc. Rev.* **2014**, *43*, 990.

(38) Suhling, K.; French, P. M. W.; Phillips, D. *Photochem. Photobiol. Sci.* **2005**, *4*, 13.

(39) Kawski, A. *Crit. Rev. Anal. Chem.* **1993**, *23*, 459.

(40) Sosa, H.; Asenjo, A. B.; Peterman, E. J. G. *Methods in Cell Biology*; Elsevier: Amsterdam, 2010; Vol. 95 (Microtubules, in vitro), p 505.

(41) Lakowicz, J. R. *Principles of Fluorescence Spectroscopy*, 3rd ed.; Springer: Berlin, 2006.

(42) Cooke, P. M. *Anal. Chem.* **2000**, *72*, 169r.

(43) Hoffmann, K.; Marlow, F.; Caro, J.; Dahne, S. *Zeolites* **1996**, *16*, 138.

(44) Megelski, S.; Lieb, A.; Pauchard, M.; Drechsler, A.; Glaus, S.; Debus, C.; Meixner, A. J.; Calzaferri, G. *J. Phys. Chem. B* **2001**, *105*, 25.

(45) Gasecka, A.; Dieu, L.-Q.; Bruhwiler, D.; S. Brasselet, S. *J. Phys. Chem. C* **2010**, *114*, 4192.

(46) Roeffaers, M. B. J.; Johan Hofkens, J.; De Cremer, G.; De Schryver, F. C.; Jacobs, P. A.; De Vos, D. E.; Sels, B. F. *Catal. Today* **2007**, *126*, 44.

(47) Busby, M.; Blum, C.; Tibben, M.; Fibikar, S.; Calzaferri, G.; Subramaniam, V.; De Cola, L. *J. Am. Chem. Soc.* **2008**, *130*, 10976.

(48) Busby, M.; Kerschbaumer, H.; Calzaferri, G.; De Cola, L. *Adv. Mater.* **2008**, *20*, 1614.

(49) Busby, M.; Devaux, A.; Blum, C.; Subramaniam, V.; Calzaferri, G.; De Cola, L. *J. Phys. Chem. C* **2011**, *115*, 5974.

(50) Huber, S.; Ruiz, A. Z.; Li, H.; Patrinoiu, G.; Botta, C.; Calzaferri, G. *Inorg. Chim. Acta* **2007**, *360*, 869.

(51) Parekh, S. H.; Domke, K. F. *Chem.—Eur. J.* **2013**, *19*, 11822.

(52) Ameloot, R.; Vermoortele, F.; Hofkens, J.; De Schryver, F. C.; De Vos, D. E.; Roeffaers, M. B. J. *Angew. Chem., Int. Ed.* **2013**, *52*, 401.

(53) Seebacher, C.; Rau, J.; Deeg, F.-W.; Brauchle, C.; Altmaier, S.; Jager, R.; Behrens, P. *Adv. Mater.* **2001**, *13*, 1374.

(54) Jung, C.; Hellriegel, C.; Platschek, B.; Wöhrle, D.; Bein, R.; Michaelis, J.; Bräuchle, C. *J. Am. Chem. Soc.* **2007**, *129*, 5570.

(55) Sheng, Q.; Ling, K.; Li, Z.; Zhao, L. *Fuel Process. Technol.* **2013**, *110*, 73.

(56) Ates, A.; Hardacre, C. *J. Colloid Interface Sci.* **2012**, *372*, 130.

(57) Aramburo, L. R.; Ruiz-Martinez, J.; Hofmann, J. P.; Weckhuysen, B. M. *Catal. Sci. Technol.* **2013**, *3*, 1208.

(58) Cairon, O. *ChemPhysChem* **2013**, *14*, 244.

(59) Mihalyi, R. M.; Kollar, M.; Kiraly, P.; Karoly, Z.; Mavrodinova, V. *Appl. Catal., A* **2012**, *417–418*, 76.

(60) Niwa, M.; Sota, S.; Katada, N. *Catal. Today* **2012**, *185*, 17.

(61) Lago, R. M.; Haag, W. O.; Mikovsky, R. J.; Olson, D. H.; Hellering, S. D.; Schmitt, K. D.; Kerr, G. T. *Stud. Surf. Sci. Catal.* **1986**, *28*, 677.

(62) Maier, S. M.; Jentys, A.; Lercher, J. A. *J. Phys. Chem. C* **2011**, *115*, 8005.

(63) Muller, J. M.; Harryvan, D. H.; Verhagen, J. C. D.; van Ginkel, G.; van Faassen, E. E. *J. Chem. Phys.* **1996**, *211*, 413.

(64) Weir, N. A.; Milkie, T. H. *J. Polym. Sci.* **1979**, *17*, 3735.

(65) Beyerlein, R. A.; Choi-Feng, C.; Hall, J. B.; Huggins, B. J.; Ray, G. J. *Top. Catal.* **1997**, *4*, 27.

(66) Buurmans, I. L. C.; Weckhuysen, B. M. *Nat. Chem.* **2012**, *4*, 873.

(67) Sambur, J. B.; Chen, P. *Annu. Rev. Phys. Chem.* **2014**, *65*, 395.

(68) Zurner, A.; Kirstein, J.; Doblinger, M.; Brauchle, C.; Bein, T. *Nature* **2007**, *450*, 705.

(69) Shim, T.; Lee, M. H.; Kim, D.; S, K. H.; Yoon, K. B. *J. Phys. Chem. B* **2009**, *113*, 966.

(70) Whiting, G. T.; Meirer, F.; Valencia, D.; Mertens, M. M.; Bons, A.-J.; Weiss, B. M.; Stevens, P. A.; de Smit, E.; Weckhuysen, B. M. *Phys. Chem. Chem. Phys.* **2014**, *16*, 24531.

(71) Zhao, Y.; D. G. Truhlar, D. G. *Theor. Chem. Acc.* **2007**, *120*, 215.

(72) Frisch, M. J.; Trucks, G. W.; Schlegel, H. B.; Scuseria, G. E.; Robb, M. A.; Cheeseman, J. R.; Scalmani, G.; Barone, V.; Mennucci, B.; Petersson, G. A.; Nakatsuji, H.; Caricato, M.; Li, X.; Hratchian, H. P.; Izmaylov, A. F.; Bloino, J.; Zheng, G.; Sonnenberg, J. L.; Hada, M.; Ehara, M.; Toyota, K.; Fukuda, R.; Hasegawa, J.; Ishida, M.; Nakajima, T.; Honda, Y.; Kitao, O.; Nakai, H.; Vreven, T.; Montgomery, Jr., J. A.; Peralta, J. E.; Ogliaro, F.; Bearpark, M.; Heyd, J. J.; Brothers, E.; Kudin,

K. N.; Staroverov, V. N.; Kobayashi, R.; Normand, J.; Raghavachari, K.; Rendell, A.; Burant, J. C.; Iyengar, S. S.; Tomasi, J.; Cossi, M.; Rega, N.; Millam, J. M.; Klene, M.; Knox, J. E.; Cross, J. B.; Bakken, V.; Adamo, C.; Jaramillo, J.; Gomperts, R.; Stratmann, R. E.; Yazyev, O.; Austin, A. J.; Cammi, R.; Pomelli, C.; Ochterski, J. W.; Martin, R. L.; Morokuma, K.; Zakrzewski, V. G.; Voth, G. A.; Salvador, P.; Dannenberg, J. J.; Dapprich, S.; Daniels, A. D.; Farkas, Ö.; Foresman, J. B.; Ortiz, J. V.; Cioslowski, J.; Fox, D. J. *Gaussian 09*, Revision B.01; Gaussian, Inc.: Wallingford CT, 2009.